Graphene oxide surface modification of polyamide reverse osmosis membranes for improved *N*-nitrosodimethylamine (NDMA) removal

Henry Croll[a,1], Adel Soroush[a,1], Makenzie E. Pillsbury[b], Santiago Romero-Vargas Castrillón[a,*]

[a] *Department of Civil, Environmental, and Geo-Engineering, University of Minnesota, Minneapolis, MN 55455, USA*
[b] *Masonic Cancer Center Mass Spectrometry Facility, University of Minnesota, Minneapolis, MN 55455, USA*

ABSTRACT

In the growing area of wastewater reuse, the performance of reverse osmosis (RO) is limited by poor membrane selectivity towards nitrosamines and other low-molecular weight, neutral contaminants. This study aimed to increase RO membrane rejection of *N*-nitrosodimethylamine (NDMA), a carcinogenic nitrosamine that is produced during chlorination and chloramination of secondary wastewater effluent. Toward this goal, we modified commercial polyamide RO membranes with graphene oxide (GO) nanosheets, and demonstrated that GO functionalization can decrease the NDMA permeability coefficient by 31%, while only decreasing water permeability by 13%. The improved selectivity is likely due to additional steric exclusion derived from the GO nanosheet coating. Moreover, membrane characterization indicated that the GO modification does not change the hydrophilicity or roughness of the interface. The latter interfacial characteristics, combined with the well-established biocidal properties of graphenic nanomaterials, render GO functionalization a promising strategy for the development of highly selective membranes for wastewater reclamation.

1. Introduction

Water scarcity is a central problem of our time. Millions of people are affected by difficult or intermittent access to drinking water, a problem that will be aggravated by population growth, industrialization, urbanization and climate change [1]. With less than 1% of available water supply in the form of drinking water, there is a clear need for technologies capable of tapping unconventional water sources (*e.g.*, brackish water, seawater, and wastewater) [2] to augment the water inventory beyond what is available from the hydrological cycle. Given their relatively low energy requirements and high pollutant removal, membrane-based processes such as reverse osmosis (RO) hold significant promise in augmenting our water supply through seawater desalination and advanced wastewater treatment [2].

The inception of the thin film composite (TFC) membrane contributed significantly to the decrease in the energy consumption of desalination and wastewater reclamation by RO [1,2]. TFC membranes [3] display high contaminant rejection (> 99% for ionic species, as well as a wide variety of micropollutants with molecular weight ≥ 150 Da [2]), and high water permeability ($2–5\,L\,m^{-2}\,h^{-1}\,bar^{-1}$ [2]) owing to a thin ($\sim 200–300\,nm$ [4]) polyamide selective layer. Conventional polyamide TFC membranes are fabricated by interfacial polymerization

(IP) of aromatic amines and acyl chlorides, typically *m*-phenylene diamine in aqueous solution and trimesoyl chloride dissolved in organic, apolar solvents [1,3,5,6]. Because IP is a stochastic, self-limiting process [5,6], the resulting active layer is a highly crosslinked glassy polymer whose chemical composition and morphology are difficult to control, and whose selectivity has proven challenging to improve. Consequently, state-of-the-art RO membranes are permeable to small, hydrophilic neutral solutes (SNSs) (*i.e.*, those with a molecular diameter similar to that of a water molecule, $\sim 0.3\,nm$), many of which are toxic [2,7–9]. Examples of SNSs which show low rejection include boron, arsenic and a host of organic disinfection byproducts (DBPs) [2,10]. The environmental and health impacts of these species range from damage in crops to cancer and developmental/reproductive effects in humans [11].

Among SNSs, the National Research Council identified *N*-nitrosodimethylamine (NDMA) (a byproduct of chloramination of secondary wastewater effluent [12,13]) as significantly concerning due to its being a potent carcinogen [14]. Different countries and regions have adopted recommendations about the presence of NDMA in drinking water: California has adopted a notification goal of $10\,ng\,L^{-1}$ for NDMA and other nitrosamines [15,16], while Germany and the Netherlands have adopted guide values of 10 and $12\,ng\,L^{-1}$, respectively, for NDMA

[16]. Concerning wastewater effluent, the regulatory level for NDMA in Ontario is $200\,ng\,L^{-1}$ [16]. Owing to its small molecular radius (0.248 nm [9]), hydrophilicity ($\log K_{ow,\ NDMA} = -0.57$, where K_{ow} is the 1-octanol/water partition coefficient [17]), and uncharged state at pH 6–8 [15], NDMA is sparsely removed by conventional membranes, with observed rejection coefficients in the 5–80% range for brackish water RO membranes [15]. Such rejection results in low RO permeate quality when the feed is impacted with wastewater disinfected with chloramines [18]. Removal of NDMA thus requires an expensive advanced oxidation process (AOP) downstream of the RO stage to degrade NDMA to less toxic compounds [2,14]. Development of a high rejection membrane would therefore reduce the capital and operating costs of advanced reuse processes, in addition to producing safer reclaimed water.

Previous research has found a strong correlation between the minimum projected area of NDMA and other neutral solutes, and their rejection by RO membranes [4], suggesting that steric hindrance derived from sub-nanometer voids in the selective layer influences contaminant transport and selectivity. Accordingly, efforts to improve the rejection of NDMA and other SNSs (e.g., boric acid) have focused on reducing the void-volume fraction through heat treatment [15,19], or via surface modification of the polyamide layer with aliphatic alkylamines [20] or monomers such as glycidyl methacrylate [7], that reduce void-volume size and disrupt solute-solvent hydrogen bonding [7,20,21]. However, the chemical moieties used in these modifications are hydrophobic [7,20], resulting in a polyamide surface with possible high organic and biological fouling propensity. Membrane surface modification with biocidal nanomaterials such as graphene oxide (GO) has proven effective in mitigating biofouling [22–24]. If, in addition, GO surface coatings could improve NDMA rejection, a valuable synergy for wastewater reuse membranes would result. However, to-date, the effect of nanomaterial surface coatings on the rejection of SNSs such as NDMA by polyamide membranes has not been explored.

In this paper we investigate the impact of GO modification on the rejection of NDMA in RO membrane filtration. We show that modifying commercial RO membranes with a GO surface coating can improve the rejection of NDMA by 6% (equivalent to a decrease in NDMA permeability coefficient of 31%) and the water/NDMA permselectivity (ratio of the permeability coefficients of water and NDMA) by 43%. The higher rejection of NDMA by GO-modified membranes is attributed to sealing of polyamide defects by GO nanosheets.

2. Materials and methods

2.1. Graphene oxide synthesis and characterization

Graphene oxide (GO) was prepared by chemical exfoliation of graphite (Bay Carbon, SP-1, 325 mesh) following the modified Hummers method [25]. A detailed description of the synthesis and material characterization can be found in our previous publication [26]. GO nanosheets were readily dispersible in ultrapure water ($18.2\,M\Omega\,cm$, Barnstead) and exhibited a mean lateral dimension (determined from scanning electron micrographs) of $\sim 80\,nm$ and thickness of $\sim 1\,nm$ (measured by tapping mode AFM), consistent with single-layer GO nanosheets [27]. Raman spectroscopy confirmed the presence of the graphite lattice in-phase vibration (G) band at $\sim 1590\,cm^{-1}$ and the disorder (D) band at $\sim 1350\,cm^{-1}$ [28].

2.2. Surface modification with graphene oxide (GO)

Polyamide thin-film composite RO membranes (SW30HR, Dow Water & Process Solutions) were provided as flat sheets and stored dry until use. Given their high rejection of other SNSs (e.g., boric acid [7,21]), seawater RO (SWRO) membranes such as SW30HR constitute a suitable material platform with which to investigate DBP removal. Before surface modification, membrane coupons were immersed in 25%

aqueous isopropanol for 30 min, and then rinsed in ultrapure water for 1 h. To functionalize the membrane surface with GO, we adapted the protocol developed by Perreault et al. [22], according to which nanosheets are tethered to polyamide via amine coupling chemistry [29] using an ethylenediamine (ED, BioXtra, Sigma) linker. Briefly, carboxylic acid groups on the polyamide active layer are converted to amine-reactive esters using EDC (1-ethyl-3-(3-dimethylaminopropyl) carbodiimide hydrochloride, 98%, Sigma) and NHS (N-hydroxysuccinimide, 98%, Sigma), at concentrations of 4 mM and 10 mM, respectively, in a 10 mM MES buffer solution (MES monohydrate, BioXtra, 99%, Sigma), pH 5.0, containing 0.5 M NaCl. After 60 min, the membrane is washed with ultrapure water and contacted with a 10 mM ED solution in 10 mM HEPES buffer (99.5%, Sigma), pH 7.5, containing 0.15 mM NaCl for 30 min; this step functionalizes the membrane surface with primary amine groups through reaction of ED with the activated esters. To activate the GO suspension, 10 parts of $250\,\mu g\,mL^{-1}$ GO suspension is combined with 2 parts 100 mM MES buffer, which is mixed with 1.75 parts 20 mM EDC (in 10 mM MES buffer) followed by 1.75 parts 50 mM NHS (in 10 mM MES buffer) to convert carboxylic acid groups that decorate the GO nanosheet edges into amine-reactive esters. The pH of EDC-NHS-activated GO dispersion is adjusted to 5.5, and after 15 min it is increased to 7.2 by the addition of NaOH dropwise. The ED-functionalized membrane is then exposed to the activated GO dispersion for 60 min, allowing reaction of the activated GO with the primary amine groups present on the membrane surface. Finally, the membrane is bath sonicated for 5 min to remove adsorbed GO, and stored at approximately 4 °C in ultrapure water until use. All membrane modifications were performed at room temperature in an orbital shaker at 30 rpm. Membrane coupons were mounted between a polypropylene backing and a PTFE frame, leaving only the polyamide active layer exposed to the modification solutions.

2.3. Characterization of membrane chemistry and interfacial properties

2.3.1. Conformal Raman mapping

Raman spectroscopy (Witec Alpha300R) was used to verify the presence and characterize the spatial distribution of GO nanosheets on the polyamide surface. Raman maps were determined over $20 \times 20\,\mu m^2$ scan areas on desiccator-dried membranes at $0.5\,\mu m$ resolution, measuring 4 spectra per square micron. To generate the GO surface density maps, we computed the ratio of the areas under the D band of GO and the polysulfone C−O−C stretching band (observed at $\sim 1150\,cm^{-1}$ [22,30]) derived from the RO membrane support.

2.3.2. Scanning electron and atomic force microscopy

Membrane surface morphology was characterized by field emission scanning electron microscopy (FESEM). The samples were sputter-coated with 5 nm of iridium (Leica EM, ACE 600) to enable SEM imaging (Hitachi SU8230). Membrane surface topography was characterized by tapping mode AFM in air using a MFP-3D-Bio AFM (Asylum Research), with AC160TS-R3 probes (Asylum Research, nominal $k = 26\,N/m$). Surface images were collected at 0.5 Hz over $2.5 \times 2.5\,\mu m^2$ areas. Root-mean-square (RMS) roughness was calculated from five AFM scans of different specimens for each membrane type.

2.3.3. Contact angle goniometry

Membrane surface hydrophobicity was characterized by the contact angle of n-decane droplets suspended in ultrapure water. The captive droplet technique allows investigation of membrane hydrophobicity in aqueous environments and circumvents artifacts due to membrane drying [31]. A goniometer (Ramé-Hart, Model 200) was used to determine the contact angles of n-decane droplets ($\sim 10\,\mu L$ volume) injected with a J-shaped needle into a fluid cell containing ultrapure water. DROP Image software (Ramé-Hart) was used to measure the contact angle of each droplet. For each membrane type, two replicate

specimens were measured for a total of 12 *n*-decane droplets.

2.3.4. Streaming potential measurements

The zeta potential of the membrane surface was determined from streaming potential measurements using an electrokinetic analyzer (SurPASS, Anton-Paar). Two membrane coupons were affixed to the sample holders of an adjustable gap cell with a gap size of 120 μm. The streaming potential was measured in 1 mM KCl from pH 10 to pH 4, adjusted with aliquots of 0.05 M HCl. The zeta potential was computed from the measured streaming potential using the Smoluchowski-Helmholtz equation [32]. For each membrane type, two separate membrane specimens were characterized.

2.4. NDMA removal efficiency

2.4.1. Analytical techniques

Samples of feed and permeate solutions were analyzed by capillary LC ESI$^+$-MS/MS with a TSQ Vantage triple quadrupole (Thermo Scientific) interfaced to a Dionex Ultimate 3000 rapid separation LC (RSLC) high performance liquid chromatography (HPLC) system (Thermo Scientific) to measure the relative amount of NDMA present in filtered water samples. Chromatographic separation was achieved using an Agilent Zorbax SB-C18 5 μm, 150 mm × 0.5 mm column. Samples were eluted at a flow rate of 15 μL/min at room temperature using 2 mM ammonium acetate with 0.1% formic acid in water and methanol with 0.1% formic acid as buffers. The column was run under isocratic conditions at 10% methanol for 9 min. NDMA elutes from the column at 4.35 min and was monitored by the selected reaction monitoring (SRM) transitions $m/z = 75.08 \rightarrow 43.13$ and $75.08 \rightarrow 58.17$. Quantitation was based on $m/z = 43.13$, while $m/z = 58.17$ was used as a qualifier ion. The instrument was operated with an electrospray ionization source with a spray voltage of 3500 kV in positive ionization mode. Nitrogen was used as the sheath and auxiliary gas (20 and 0.5 units, respectively), and the ion transfer tube was set to 350 °C. Argon was used as the collision gas, and set to 1.0 mTorr. For $m/z = 43.13$, a collision energy of 16 V was used, and for $m/z = 58.17$ a collision energy of 12 V was used. The S-Lens of the instrument was set to 40 V, and a declustering voltage of 10 V was used. Quadrupole resolution was achieved at 0.7 (FWHM) for both Q1 and Q3. A sample chromatogram is given in Fig. S1 of the Appendix. Prepared synthetic standards over the expected concentration range were injected to create a standard curve. Sample NDMA concentration was determined from the measured peak area using the standard curve.

Supplementary data associated with this article can be found, in the online version, at https://doi.org/10.1016/j.seppur.2018.08.070.

2.4.2. Membrane filtration system

A laboratory-scale RO filtration apparatus was employed, consisting of a crossflow cell (CF042D, Sterlitech) with a membrane active area of 42.1 cm^2, high-pressure pump (HydraCell M-03S, Wanner Engineering), 19-L stainless steel feed reservoir and heat exchange coil (Sterlitech) and chiller unit (6500 Series, PolyScience). The permeate flow rate was recorded by either a digital flow meter (SLI, Sensirion) connected to a computer, or by measuring the permeate volume as a function of time (in the latter case, good agreement was found with data recorded by the digital flow meter).

2.4.3. Characterization of NDMA rejection

Membranes were tested in ultrapure water supplemented with NDMA at a concentration of 890 μg L^{-1} (dosed from a 1.35 M NDMA stock solution, prepared in water from neat NDMA (Supelco, Sigma Aldrich)). This elevated feed concentration was chosen because it facilitates direct analysis by LC-MS/MS without the need for sample concentration. Moreover, we carried out two additional experiments to investigate the effect of feed concentration on rejection with control membranes. Experiments at higher feed concentration (1125 μg L^{-1}, $R_{NDMA} = 84.9\%$) and lower feed concentration (462 μg L^{-1}, $R_{NDMA} = 82.2\%$) showed no apparent effect on NDMA removal, in agreement with previous work [33]. All experiments were conducted at a feed temperature of 22 °C and a crossflow velocity $u = 0.08 \, \text{m s}^{-1}$. Under these conditions, $Re = ud_H/\upsilon = 363$, where $d_H = 4.38 \times 10^{-3} \, \text{m}$ is the hydraulic diameter of the crossflow channel and υ is the kinematic viscosity of water at 22 °C, equal to $9.57 \times 10^{-7} \, \text{m}^2 \, \text{s}^{-1}$. The pH of the feed solution was ~5.8–6.2, conditions under which NDMA is uncharged [15]. The permeate flux was first allowed to reach steady state by compacting the membrane at 400 psi with an ultrapure water feed. Following compaction, NDMA was dosed to the feed tank. After allowing at least 2 h for the solute to attain adsorption equilibrium with the membrane, 3 feed and 3 permeate samples were collected in 300 μL glass vials and stored in the dark at approximately 4 °C until analysis by LC-MS/MS was conducted.

The intrinsic water permeability (A) was determined by dividing the permeate flux (J_w) by the transmembrane pressure difference (Δp). NDMA separation was quantified by the rejection coefficient $R_{NDMA} = 1 - C_p/C_f$, where C_p and C_f are the bulk permeate and feed NDMA concentrations. Reported values of R_{NDMA} represent the average of three measurements. The permeability coefficient of NDMA (B) was computed from

$$B = J_w \left(\frac{1 - R_{NDMA}}{R_{NDMA}} \right) \exp\left(-\frac{J_w}{k} \right) \tag{1}$$

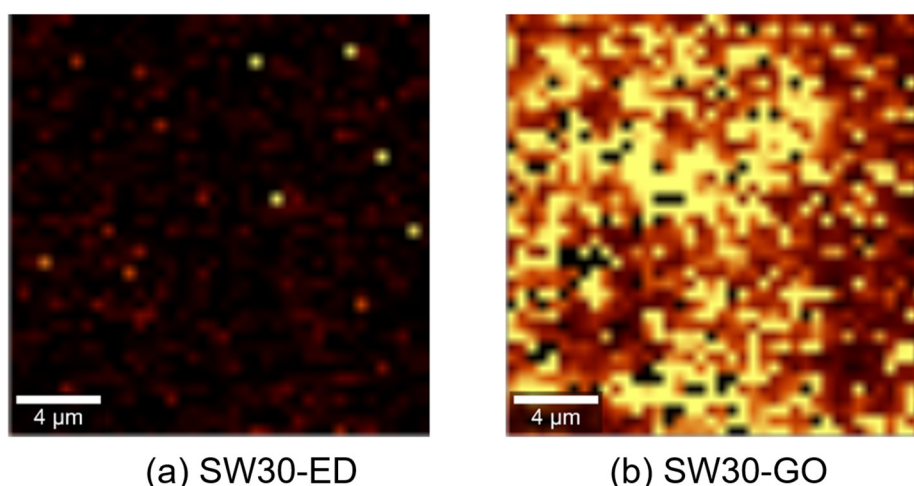$$(a) \, \text{SW30-ED} \qquad (b) \, \text{SW30-GO}$$

Fig. 1. Raman spectroscopy maps of (a) ethylenediamine (ED)-modified (SW30-ED) and (b) GO-functionalized (SW30-GO) polyamide membrane surfaces.

where k is the mass transfer coefficient, calculated from the correlation for the Sherwood number ($Sh = k d_H / D$, where $D = 9.9 \times 10^{-10} \, \text{m}^2 \, \text{s}^{-1}$ is the aqueous diffusivity of NDMA [33]) under laminar flow in thin rectangular channels without spacers [34],

$$Sh = 1.85 (ReScd_H/L)^{0.33} \tag{2}$$

where $Sc = \upsilon/D$ is the Schmidt number and $L = 9.2 \times 10^{-2} \, \text{m}$ is the length of the crossflow channel.

2.5. Statistical analysis

Homoscedastic (equal variance) unpaired *t*-tests were performed using Microsoft Excel to determine the statistical significance of the results. To evaluate the removal of NDMA by the different membrane materials, we considered seven membrane specimens independently functionalized with GO (hereinafter referred to as SW30-GO). In addition, we characterized NDMA rejection of six control membranes (designated as SW30), and two membranes functionalized with ED (designated SW30-ED). Error estimates in NDMA rejection coefficient are given as the standard deviation of three different measurements.

3. Results and discussion

3.1. Membrane material characterization

3.1.1. Raman spectroscopy and electron microscopy

We assessed the extent of membrane surface functionalization with GO by means of confocal Raman mapping. The results are presented in Fig. 1. The Raman map corresponding to the SW30-GO membrane (Fig. 1(b)) exhibits regions of high brightness (whose intensity is proportional to the ratio of the D band in GO to the polysulfone band), thus confirming successful functionalization with GO. The heterogeneity in the coverage observed in Fig. 1(b) is likely due to the broad sheet size distribution observed in the synthesized GO, with sheet lateral dimensions varying by one order of magnitude [26]. Conversely, no GO signatures are observed in the GO-free SW30-ED membrane (Fig. 1(a)).

Similarly, electron micrographs presented in Fig. 2 confirm the presence of GO as a crumpled sheet-like nanomaterial overlaying the polyamide (Fig. 2(b)), or as darker regions over the polyamide (Fig. 2(d)); these morphological features are absent in the SW30 control

(Fig. 2(a) and (c)), which shows the well-known leaf-like structure of polyamide [35]. The features noted in the micrographs of Fig. 2 are consistent with those reported previously by others in similar systems [22,23].

3.1.2. Interfacial properties

The effect of GO functionalization on surface roughness and membrane wettability is explored in Figs. 3 and 4, respectively, using atomic force microscopy (AFM) and contact angle goniometry. The AFM image corresponding to SW30 (Fig. 3(a)) exhibits the familiar ridge-and-valley structure of polyamide [5,36]. A seemingly different morphology is exhibited by the SW30-GO specimen (Fig. 3(b)), with smoother domains that are possibly due to GO nanosheets covering the rougher features of polyamide. These differences, however, are not reflected in the root-mean-squared roughness, which demonstrated similar values for both types of membranes: $60.2 \pm 9.7 \, \text{nm}$ for SW30 and $58.8 \pm 7.3 \, \text{nm}$ for SW30-GO ($p = 0.82$).

Fig. 4 presents results on the wettability of the membrane surfaces by a hydrophobic organic liquid, characterized by the contact angle of captive *n*-decane droplets in ultrapure water. With contact angles $> 90°$ (measured through the *n*-decane droplet), the results show that both membrane interfaces were poorly wetted by *n*-decane. On closer inspection, we observe a slightly larger contact angle in SW30-GO ($164.0°$ compared to $161.2°$ for SW30, $p = 0.008$), suggesting that GO surface modification results in a somewhat more hydrophilic interface compared to the control, a result that can be attributed to the hydrophilicity of GO films [26]. The results in Figs. 3 and 4 therefore show that GO functionalization does not render the membrane surface more hydrophobic nor does it increase surface roughness, both of which are desirable features from the point of view of fouling control [37,38].

To elucidate the effect of GO functionalization on membrane charge, we determined the ζ-potential of the membrane surfaces by means of streaming potential measurements. The results are presented in Fig. 5. Control (SW30) and ED-functionalized membranes (SW30-ED) exhibited no discernible differences in charging behavior in the pH 4–10 range, the surface charge becoming more negative as pH increases, due to deprotonation of carboxylic acid functional groups [39]. In contrast, a significant increase in surface charge was observed in SW30-GO membrane specimens, with the zeta potential increasing (in absolute value terms) by ∼25 mV at circumneutral pH relative to the
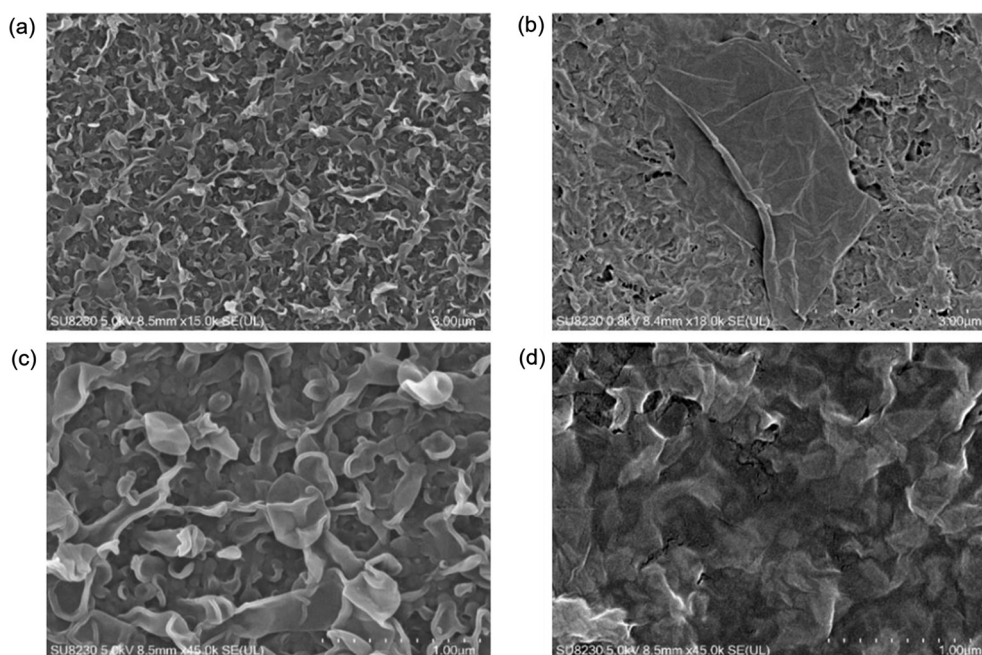

Fig. 2. Scanning electron micrographs of (a, c) control (SW30) and (b, d) GO-functionalized (SW30-GO) polyamide membrane surfaces.
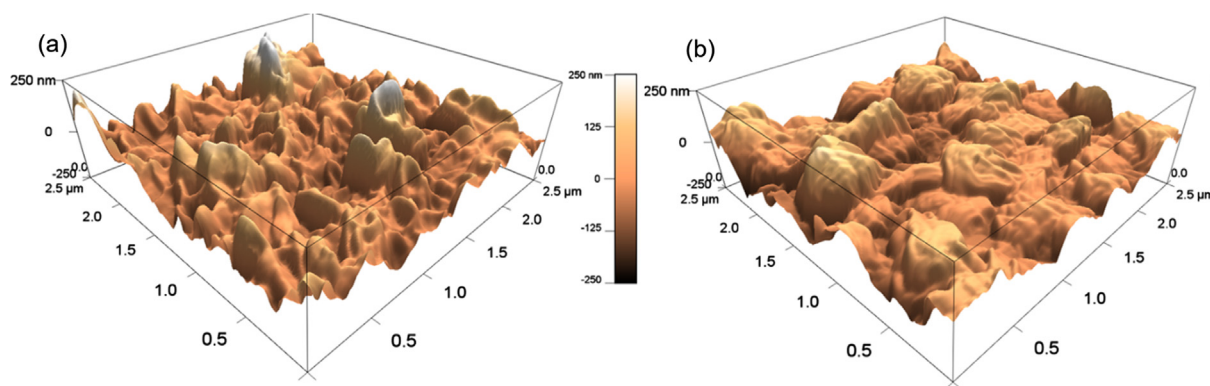
Fig. 3. Tapping mode AFM images of (a) control (SW30) and (b) GO-functionalized (SW30-GO) polyamide membrane surfaces.
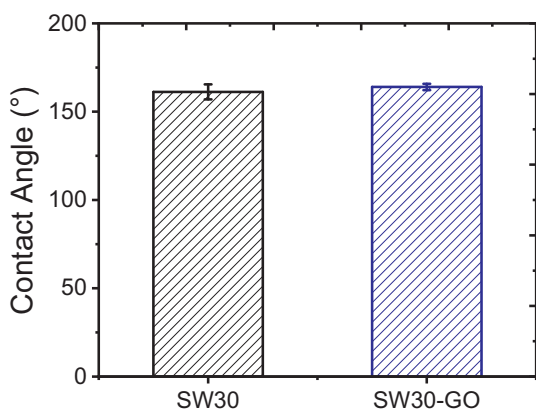

Fig. 4. Contact angles obtained through the captive bubble method using *n*-decane droplets in ultrapure water. The average of 12 *n*-decane droplets recorded over two membrane specimens of each type is shown. Error bars denote one standard deviation.
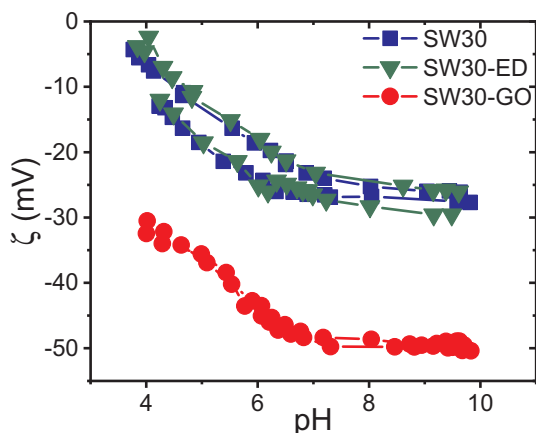

Fig. 6. Average NDMA permeability coefficient (B_{av}) and average NDMA rejection coefficient ($R_{NDMA, av}$) of control (SW30) and GO-functionalized (SW30-GO) polyamide membranes. The results shown are averages of six SW30 and seven SW30-GO membrane coupons. Error bars indicate one standard deviation.

3.2. Effect of GO surface functionalization on NDMA rejection

Figs. 6 and 7 present the average water permeability coefficient (A_{av}), average NDMA permeability coefficient (B_{av}), and average NDMA rejection coefficient ($R_{NDMA, av}$), obtained from six SW30 filtration experiments and seven filtration experiments with independently functionalized SW30-GO membrane samples. In addition, Fig. 7 presents the average water/NDMA permselectivity, $(A/B)_{av}$.

Fig. 5. ζ-potential of control (SW30), ethylenediamine-modified (SW30-ED), and GO-functionalized (SW30-GO) polyamide membranes over the pH range 4–10. Measurements were performed in a 1 mM KCl background electrolyte. Results are shown for two samples of each membrane type.

control and ED-functionalized surfaces. We attribute the increase in negative charge of the membrane surface to a higher surface density of carboxylate functional groups derived from the GO nanosheets [40,41]. A similar increase in the negative charge of polyamide membranes after GO modification has been reported by others [42,43]. These results provide further confirmation of the successful functionalization of the membrane surfaces with GO.
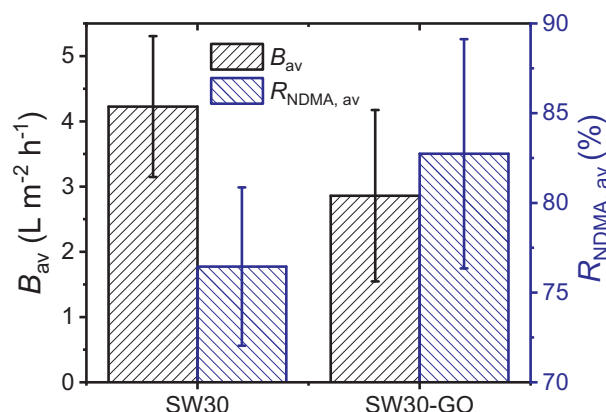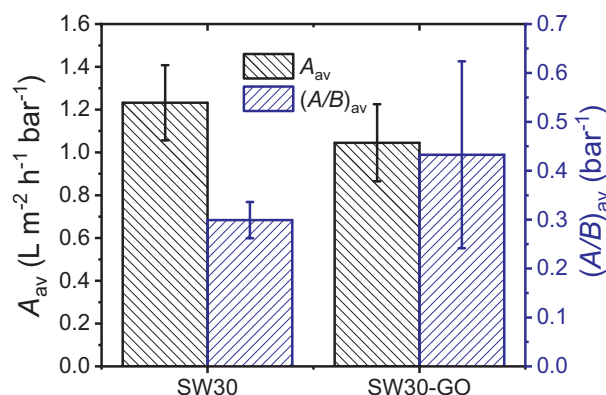

Fig. 7. Average water permeability coefficient (A_{av}) and average water/NDMA permselectivity ($(A/B)_{av}$) of control (SW30) and GO-functionalized (SW30-GO) polyamide membranes. The results shown are averages of six SW30 and seven SW30-GO membrane coupons. Error bars indicate one standard deviation.

Fig. 6 demonstrates that GO surface modification improves NDMA rejection ($R_{NDMA,\ av}$) by 6.2%, increasing from 76.5% for SW30 to 82.7% for SW30-GO ($p = 0.068$). The improved removal of NDMA is similarly manifested by a decrease in B_{av} from 4.2 L m^{-2} h^{-1} (LMH) for SW30 to 2.9 LMH for SW30-GO ($p = 0.068$). We further investigated the role of the ED linker in NDMA removal: the NDMA rejection coefficient of SW30-ED, 80.2%, showed that ethylenediamine plays a role in NDMA rejection, though additional gains in nitrosamine removal are due to the combined ED-GO surface modification. SW30-GO membranes will thus be the focus of the discussion that follows.

Fig. 7 shows that improved rejection is observed at the expense of a 13% decrease in water permeability, with A_{av} decreasing from 1.2 LMH bar^{-1} for SW30 (a value consistent with that specified by the manufacturer, *i.e.*, 1.1 LMH bar^{-1}) to 1.05 LMH bar^{-1} (SW30-GO) ($p = 0.086$). The observed decrease in water permeability is due to the additional hydraulic resistance derived from the GO layer, and reflects the well-known tradeoff between water permeability and membrane separation performance [2,15,44]. We note that the decrease in A_{av} is smaller than that observed following heat treatment (20–35%) [15], a strategy pursued by others to achieve high (92%) nitrosamine removal, albeit with significant loss of water permeance [15]. Moreover, improved NDMA rejection observed with GO functionalization results in improved water/NDMA permselectivity, $(A/B)_{av}$, which increases from 0.3 bar^{-1} to 0.43 bar^{-1} ($p = 0.12$) following GO surface modification, as shown in Fig. 7.

Figs. 8 and 9 present the results of the individual filtration experiments from which the average quantities in Figs. 6 and 7 were computed. We observe significant variability in membrane transport properties across SW30 and SW30-GO coupons, which is nonetheless within the expected range specified by the manufacturer ($\pm 15\%$ [45]). Variation in transport properties across specimens of the same membrane type is a common feature of polyamide membrane materials [20,46]. For control membranes, the variability in transport properties and selectivity is likely due to regions in SW30HR polyamide that possess different chemical compositions. As observed by others [21], SW30HR polyamide exhibits nitrogen-rich regions (comprising ~ 8–10% N and $\leq 20\%$ O), and nitrogen-poor regions (1–3% N and 24–33% O) indicative of a proprietary surface coating that does not uniformly cover polyamide [21,47–50].

For the six control (SW30) coupons investigated, A varies from 1 LMH bar^{-1} to 1.4 LMH bar^{-1}. Within this range, NDMA rejection decreases from 81% to 72% (Fig. 8); similarly, the NDMA permeability coefficient (B) is shown to increase from 3.1 LMH to 5.3 LMH as A
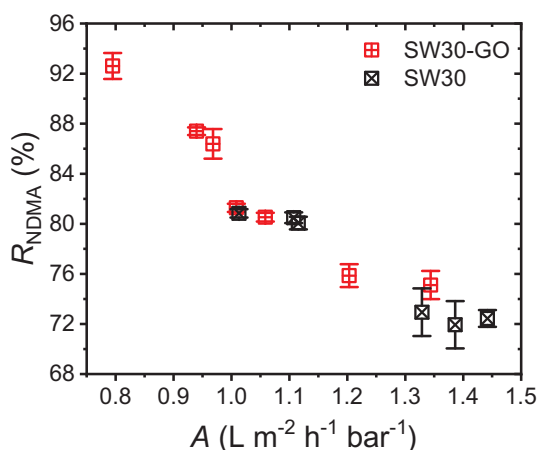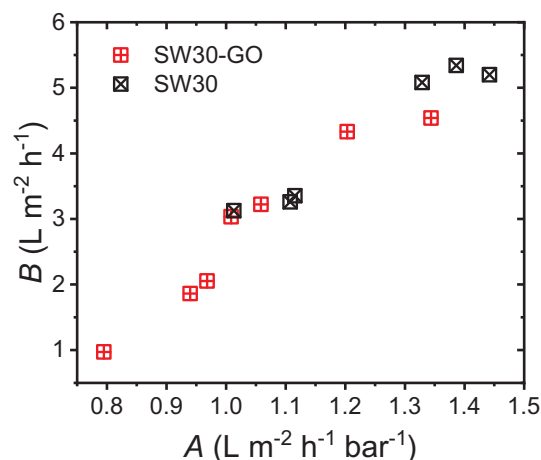
Fig. 9. Dependence of NDMA permeability coefficient (B) on water permeability coefficient (A) for individual membrane filtration experiments with control (SW30) and GO-functionalized (SW30-GO) membrane specimens.

increases (Fig. 9), *i.e.*, the observed dependence of R_{NDMA} and B on A is consistent with the permeability-selectivity tradeoff. Similar variability is observed across individual GO-modified membrane specimens; this variation can be attributed to the chemically distinct regions of the underlying polyamide layer, and is possibly compounded by a somewhat heterogeneous GO coating (observe the GO-lean regions in the Raman maps shown in Fig. 1). Accordingly, NDMA removal is observed to decrease from 93% to 75% (equivalent to an increase in B from 1.0 LMH to 4.5 LMH) as the water permeability coefficient increases from 0.8 to 1.3 LMH bar^{-1}.

Contaminant removal by reverse osmosis is derived from multiple physical and chemical properties of the membranes: surface chemistry (*i.e.*, hydrophobicity or hydrophilicity) affects contaminant partitioning into the membrane [7,21,51]; further, membrane surface charge strongly influences rejection of charged species through Donnan exclusion [52]; finally, nanoscale voids in polyamide modulate water and contaminant transport across the polymer film [4,9]. Membrane hydrophobicity and charge do not explain the increase of NDMA rejection observed above with SW30-GO membranes, given that NDMA is uncharged at circumneutral pH [15], rendering Donnan exclusion inoperable. Moreover, SW30 and SW30-GO specimens showed similar wetting by *n*-decane (Fig. 4), suggesting that the GO coating does not noticeably affect hydrophilicity and NDMA partitioning. On the other hand, the observation that the highest NDMA rejection is exhibited by membrane specimens with relatively low A (Fig. 8) suggests that the improved NDMA removal observed in GO-functionalized membranes may be due to obstruction of nanoscale defects in polyamide by the ED-mediated tethering of GO nanosheets. Defects in polyamide, present as free-volume cavities ~ 0.27 nm in radius [4], are blocked by the covalently bonded layer of GO nanosheets, which are themselves impermeable to water and solutes [53,54], leading to improved removal of NDMA by steric exclusion.

4. Concluding remarks

Development of membranes demonstrating high rejection of SNSs remains a long-standing challenge in membrane separations. Focusing on NDMA, a carcinogenic SNS of significant concern in wastewater reclamation, we have shown that surface functionalization of commercial polyamide membranes with GO nanosheets – a building block of membrane biocidal coatings – results in improved NDMA rejection. We draw the following conclusions from our study:

- Compared to control membranes, GO-functionalized (SW30-GO)

Fig. 8. Dependence of NDMA rejection coefficient (R_{NDMA}) on water permeability coefficient (A) for individual membrane filtration experiments with control (SW30) and GO-functionalized (SW30-GO) membrane specimens. R_{NDMA} denotes the mean rejection based on three feed and permeate samples (error bars indicate one standard deviation).

membranes improve NDMA rejection by 6.2%, increasing from 76.5% to 82.7%. We ascribe the improvement in NDMA removal to sealing of defects in polyamide by the covalently bonded GO layer.

- The improved NDMA rejection occurs at the expense of a 13% decrease in water permeability coefficient, due to the higher hydraulic resistance caused by the GO layer. Nevertheless, the loss of water permeance appears to be moderate, given that an increase in the water/NDMA permselectivity from $0.3\,\mathrm{bar}^{-1}$ to $0.43\,\mathrm{bar}^{-1}$ is also observed.

- In contrast with other surface modification strategies, membrane functionalization with GO does not negatively alter the interfacial properties of the polyamide (notably hydrophobicity and roughness), making this a promising strategy for the modification of membranes for wastewater reclamation.

Acknowledgements

References

[1] M. Elimelech, W.A. Phillip, The future of seawater desalination: energy, technology, and the environment, Science 333 (2011) 712–717, https://doi.org/10.1126/science.1200488.

[2] J.R. Werber, A. Deshmukh, M. Elimelech, The critical need for increased selectivity, not increased water permeability, for desalination membranes, Environ. Sci. Technol. Lett. 3 (2016) 112–120, https://doi.org/10.1021/acs.estlett.6b00050.

[3] R.J. Petersen, Composite reverse osmosis and nanofiltration membranes, J. Memb. Sci. 83 (1993) 81–150, https://doi.org/10.1016/0376-7388(93)80014-O.

[4] T. Fujioka, B.E. O'Rourke, K. Michishio, Y. Kobayashi, N. Oshima, H. Kodamatani, T. Shintani, L.D. Nghiem, Transport of small and neutral solutes through reverse osmosis membranes: role of skin layer conformation of the polyamide film, J. Memb. Sci. 554 (2018) 301–308.

[5] V. Freger, Kinetics of film formation by interfacial polycondensation, Langmuir 21 (2005) 1884–1894, https://doi.org/10.1021/la048085v.

[6] V. Freger, S. Srebnik, Mathematical model of charge and density distributions in interfacial polymerization of thin films, J. Appl. Polym. Sci. 88 (2003) 1162–1169, https://doi.org/10.1002/app.11716.

[7] R. Bernstein, S. Belfer, V. Freger, Toward improved boron removal in RO by membrane modification: feasibility and challenges, Environ. Sci. Technol. 45 (2011) 3613–3620, https://doi.org/10.1021/es103991u.

[8] V.S. Freger, H. Shemer, A.A. Sagiv, R.R. Semiat, Boron removal using membranes, Boron Sep. Process. (2015) 199–217, https://doi.org/10.1016/B978-0-444-63454-2.00008-3.

[9] H. Takeuchi, H. Tanaka, L.D. Nghiem, T. Fujioka, Emerging investigators series: a steric pore-flow model to predict the transport of small and uncharged solutes through a reverse osmosis membrane, Environ. Sci. Water Res. Technol. (2018), https://doi.org/10.1039/C7EW00194K.

[10] G.M. Geise, H.S. Lee, D.J. Miller, B.D. Freeman, J.E. McGrath, D.R. Paul, Water purification by membranes: the role of polymer science, J. Polym. Sci. Part B Polym. Phys. 48 (2010) 1685–1718, https://doi.org/10.1002/polb.22037.

[11] L.F. Greenlee, D.F. Lawler, B.D. Freeman, B. Marrot, P. Moulin, Reverse osmosis desalination: water sources, technology, and today's challenges, Water Res. 43 (2009) 2317–2348, https://doi.org/10.1016/j.watres.2009.03.010.

[12] T. Fujioka, H. Kodamatani, H. Aizawa, S. Gray, K.P. Ishida, L.D. Nghiem, Role of membrane fouling substances on the rejection of N-nitrosamines by reverse osmosis, Water Res. 118 (2017) 187–195, https://doi.org/10.1016/j.watres.2017.03.057.

[13] A.D. Shah, W.A. Mitch, Halonitroalkanes, halonitriles, haloamides, and N-nitrosamines: a critical review of nitrogenous disinfection byproduct formation pathways, Environ. Sci. Technol. 46 (2012) 119–131, https://doi.org/10.1021/es203312s.

[14] Committee on the Assessment of Water Reuse as an Approach to Meeting Future Water Supply Needs; National Research Council, Water reuse: potential for expanding the nation's water supply through reuse of municipal wastewater, Natl. Acad. Press, 2012, http://doi.org/10.17226/13303.

[15] T. Fujioka, K.P. Ishida, T. Shintani, H. Kodamatani, High rejection reverse osmosis membrane for removal of N-nitrosamines and their precursors, Water Res. 131 (2018) 45–51, https://doi.org/10.1016/j.watres.2017.12.025.

[16] C. Planas, Ó. Palacios, F. Ventura, J. Rivera, J. Caixach, Analysis of nitrosamines in water by automated SPE and isotope dilution GC/HRMS. Occurrence in the different steps of a drinking water treatment plant, and in chlorinated samples from a reservoir and a sewage treatment plant effluent, Talanta (2008), https://doi.org/10.1016/j.talanta.2008.04.060.

[17] ATSDR, Toxicological Profile for N-nitrosodimethylamine, December 1989.

[18] D. Kim, G.L. Amy, T. Karanfil, Disinfection by-product formation during seawater desalination: a review, Water Res. 81 (2015) 343–355, https://doi.org/10.1016/j.watres.2015.05.040.

[19] T. Fujioka, N. Oshima, R. Suzuki, M. Higgins, W.E. Price, R.K. Henderson, L.D. Nghiem, Effect of heat treatment on fouling resistance and the rejection of small and neutral solutes by reverse osmosis membranes, Water Sci. Technol. Water Supply 15 (2015) 510–516, https://doi.org/10.2166/ws.2014.135.

[20] S. Shultz, M. Bass, R. Semiat, V. Freger, Modification of polyamide membranes by hydrophobic molecular plugs for improved boron rejection, J. Memb. Sci. 546 (2018) 165–172, https://doi.org/10.1016/j.memsci.2017.10.003.

[21] S. Shultz, V. Freger, In situ modification of membrane elements for improved boron rejection in RO desalination, Desalination (2017), https://doi.org/10.1016/j.desal.2017.08.021.

[22] F. Perreault, M.E. Tousley, M. Elimelech, Thin-film composite polyamide membranes functionalized with biocidal graphene oxide nanosheets, Environ. Sci. Technol. Lett. 1 (2013) 71–76, https://doi.org/10.1021/ez4001356.

[23] F. Perreault, H. Jaramillo, M. Xie, M. Ude, L.D. Nghiem, M. Elimelech, Biofouling mitigation in forward osmosis using graphene oxide functionalized thin-film composite membranes, Environ. Sci. Technol. 50 (2016) 5840–5848, https://doi.org/10.1021/acs.est.5b06364.

[24] A. Soroush, W. Ma, M. Cyr, M.S. Rahaman, B. Asadishad, N. Tufenkji, In situ silver decoration on graphene oxide-treated thin film composite forward osmosis membranes: biocidal properties and regeneration potential, Environ. Sci. Technol. Lett. 3 (2016) 13–18, https://doi.org/10.1021/acs.estlett.5b00304.

[25] V.C. Tung, M.J. Allen, Y. Yang, R.B. Kaner, High-throughput solution processing of large-scale graphene, Nat. Nanotechnol. 4 (2009) 25–29, https://doi.org/10.1038/nnano.2008.329.

[26] J. Xue, S. BinAhmed, Z. Wang, N.G. Karp, B.L. Stottrup, S. Romero-Vargas Castrillón, Bacterial adhesion to graphene oxide (GO)-functionalized interfaces is determined by hydrophobicity and GO sheet spatial orientation, Environ. Sci. Technol. Lett. 5 (2018) 14–19.

[27] G. Eda, G. Fanchini, M. Chhowalla, Large-area ultrathin films of reduced graphene oxide as a transparent and flexible electronic material, Nat. Nanotechnol. 3 (2008) 270–274, https://doi.org/10.1038/nnano.2008.83.

[28] K.N. Kudin, B. Ozbas, H.C. Schniepp, R.K. Prud'homme, I.A. Aksay, R. Car, Raman spectra of graphite oxide and functionalized graphene sheets, Nano Lett. 8 (2008) 36–41, https://doi.org/10.1021/nl071822y.

[29] Z. Grabarek, J. Gergely, Zero-length crosslinking procedure with the use of active esters, Anal. Biochem. 185 (1990) 131–135, https://doi.org/10.1016/0003-2697(90)90267-D.

[30] H.J. Kim, A.E. Fouda, K. Jonasson, In situ study on kinetic behavior during asymmetric membrane formation via phase inversion process using Raman spectroscopy, J. Appl. Polym. Sci. 75 (2000) 135–141, https://doi.org/10.1002/(SICI)1097-4628(20000103)75:1<135::AID-APP15>3.0.CO;2-9.

[31] W. Zhang, B. Hallström, Membrane characterization using the contact angle technique I. Methodology of the captive bubble technique, Desalination (1990), https://doi.org/10.1016/0011-9164(90)80067-L.

[32] S.L. Walker, S. Bhattacharjee, E.M.V. Hoek, M. Elimelech, A novel asymmetric clamping cell for measuring streaming potential of flat surfaces, Langmuir 18 (2002) 2193–2198, https://doi.org/10.1021/la011284j.

[33] Y. Miyashita, S. Park, H. Hyung, C.-H. Huang, J.-H. Kim, Removal of N-nitrosamines and their precursors by nanofiltration and reverse osmosis membranes, J. Environ. Eng. 135 (2009) 788–795, https://doi.org/10.1061/(ASCE)EE.1943-7870.0000043.

[34] G. Schock, A. Miquel, Mass transfer and pressure loss in spiral wound modules, Desalination 64 (1987) 339–352, https://doi.org/10.1016/0011-9164(87)90107-X.

[35] X. Lu, L.H. Arias Chavez, S. Romero-Vargas Castrillón, J. Ma, M. Elimelech, Influence of active layer and support layer surface structures on organic fouling propensity of thin-film composite forward osmosis membranes, Environ. Sci. Technol. 49 (2015) 1436–1444, https://doi.org/10.1021/es5044062.

[36] C.Y. Tang, Y.N. Kwon, J.O. Leckie, Effect of membrane chemistry and coating layer on physiochemical properties of thin film composite polyamide RO and NF membranes. II. Membrane physiochemical properties and their dependence on polyamide and coating layers, Desalination 242 (2009) 168–182, https://doi.org/10.1016/j.desal.2008.04.004.

[37] A. Tiraferri, Y. Kang, E.P. Giannelis, M. Elimelech, Superhydrophilic thin-film composite forward osmosis membranes for organic fouling control: fouling behavior and antifouling mechanisms, Environ. Sci. Technol. 46 (2012) 11135–11144, https://doi.org/10.1021/es3028617.

[38] E.M. Vrijenhoek, S. Hong, M. Elimelech, Influence of membrane surface properties on initial rate of colloidal fouling of reverse osmosis and nanofiltration membranes, J. Memb. Sci. 188 (2001) 115–128, https://doi.org/10.1016/S0376-7388(01)00376-3.

[39] A.E. Childress, M. Elimelech, Effect of solution chemistry on the surface charge of polymeric reverse osmosis and nanofiltration membranes, J. Memb. Sci. 119 (1996) 253–268, https://doi.org/10.1016/0376-7388(96)00127-5.

[40] V.C. Sanchez, A. Jachak, R.H. Hurt, A.B. Kane, Biological interactions of graphene-family nanomaterials: an interdisciplinary review, Chem. Res. Toxicol. 25 (2012) 15–34, https://doi.org/10.1021/tx200339h.

[41] D. Li, M.B. Müller, S. Gilje, R.B. Kaner, G.G. Wallace, Processable aqueous dispersions of graphene nanosheets, Nat. Nanotechnol. 3 (2008) 101–105, https://doi.

org/10.1038/nnano.2007.451.

[42] L. He, L.F. Dumée, C. Feng, L. Velleman, R. Reis, F. She, W. Gao, L. Kong, Promoted water transport across graphene oxide-poly(amide) thin film composite membranes and their antibacterial activity, Desalination (2015), https://doi.org/10.1016/j.desal.2015.02.032.

[43] H.R. Chae, J. Lee, C.H. Lee, I.C. Kim, P.K. Park, Graphene oxide-embedded thin-film composite reverse osmosis membrane with high flux, anti-biofouling, and chlorine resistance, J. Memb. Sci. (2015), https://doi.org/10.1016/j.memsci.2015.02.045.

[44] G.M. Geise, H.B. Park, A.C. Sagle, B.D. Freeman, J.E. McGrath, Water permeability and water/salt selectivity tradeoff in polymers for desalination, J. Memb. Sci. 369 (2011) 130–138, https://doi.org/10.1016/j.memsci.2010.11.054.

[45] DOW Filmtec SW30HR-380 Element Product Data Sheet (n.d.), < https://www.dow.com/en-us/markets-and-solutions/products/DOWFILMTECSeawaterReverseOsmosis8Elements/DOWFILMTECSW30HR380 > .

[46] A.C. Sagle, E.M. Van Wagner, H. Ju, B.D. McCloskey, B.D. Freeman, M.M. Sharma, PEG-coated reverse osmosis membranes: desalination properties and fouling resistance, J. Memb. Sci. (2009), https://doi.org/10.1016/j.memsci.2009.05.013.

[47] C.Y. Tang, Y.N. Kwon, J.O. Leckie, Probing the nano- and micro-scales of reverse osmosis membranes-A comprehensive characterization of physiochemical properties of uncoated and coated membranes by XPS, TEM, ATR-FTIR, and streaming potential measurements, J. Memb. Sci. 287 (2007) 146–156, https://doi.org/10.1016/j.memsci.2006.10.038.

[48] C. Wang, G.K. Such, A. Widjaya, H. Lomas, G. Stevens, F. Caruso, S.E. Kentish, Click poly(ethylene glycol) multilayers on RO membranes: fouling reduction and membrane characterization, J. Memb. Sci. 409–410 (2012) 9–15, https://doi.org/10.1016/j.memsci.2012.02.049.

[49] A. Widjaya, T. Hoang, G.W. Stevens, S.E. Kentish, A comparison of commercial reverse osmosis membrane characteristics and performance under alginate fouling conditions, Sep. Purif. Technol. 89 (2012) 270–281, https://doi.org/10.1016/j.seppur.2012.01.038.

[50] V.T. Do, C.Y. Tang, M. Reinhard, J.O. Leckie, Degradation of polyamide nanofiltration and reverse osmosis membranes by hypochlorite, Environ. Sci. Technol. 46 (2012) 852–859, https://doi.org/10.1021/es203090y.

[51] A. Ben-David, Y. Oren, V. Freger, Thermodynamic factors in partitioning and rejection of organic compounds by polyamide composite membranes, Environ. Sci. Technol. 40 (2006) 7023–7028, https://doi.org/10.1021/es0609912.

[52] S. Lee, R.M. Lueptow, Membrane rejection of nitrogen compounds, Environ. Sci. Technol. 35 (2001) 3008–3018, https://doi.org/10.1021/es0018724.

[53] Y. Su, V.G. Kravets, S.L. Wong, J. Waters, A.K. Geim, R.R. Nair, Impermeable barrier films and protective coatings based on reduced graphene oxide, Nat. Commun. (2014), https://doi.org/10.1038/ncomms5843.

[54] J.S. Bunch, S.S. Verbridge, J.S. Alden, A.M. Van Der Zande, J.M. Parpia, H.G. Craighead, P.L. McEuen, Impermeable atomic membranes from graphene sheets, Nano Lett. (2008), https://doi.org/10.1021/nl801457b.

Graphene Oxide Surface Modification of Polyamide Reverse Osmosis Membranes

for Improved *N*-Nitrosodimethylamine (NDMA) Removal

Henry Croll[1,♦], Adel Soroush[1,♦], Makenzie E. Pillsbury[2], Santiago Romero-Vargas Castrillón[1*]

[1] Department of Civil, Environmental, and Geo- Engineering, University of Minnesota, Minneapolis, MN 55455, USA

[2] Masonic Cancer Center Mass Spectrometry Facility, University of Minnesota, Minneapolis, MN 55455, USA

♦These authors contributed equally to this work

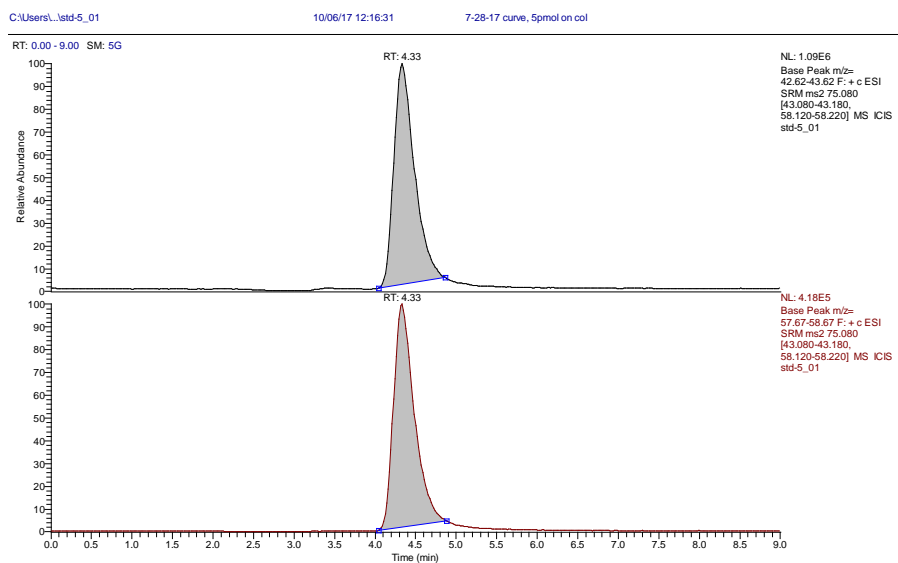*Corresponding author: sromerov@umn.edu. Tel.: +1 (612) 301-1347

Figure S1. Chromatogram of a synthetic standard mixture (5 pmol injected into column). The top image corresponds to the quantitative channel, while the bottom image is that of the qualifier ion.